Journal of Materials Chemistry C

ARTICLE

An AIE-active phosphorescent Ir(III) complex with piezochromic luminescence (PCL) and its application for monitoring volatile organic compounds (VOCs)

Yang Jiang,[a] Guangfu Li,[a] Dongxia Zhu,*[a] Zhongmin Su*[a] and Martin R. Bryce*[b]

A neutral multifunctional dinuclear Ir(III) complex **1** with a Schiff base bridging ligand is shown to combine aggregation-induced emission (AIE), piezochromic luminescence (PCL) and vapochromism. The complex displays a reversible colour change in its phosphorescence in the solid state between faint red and bright orange with high contrast intensity, triggered by high polarity volatile organic compounds (VOCs) or by mechanical grinding within 10 s. Notably, unlike many known vapochromic systems, complex **1** exhibits ultrahigh stability, with the orange colour remaining unchanged in air for several months at room temperature. A simple and efficient monitoring device has been fabricated in which highly polar VOCs act as a switch to "turn on" the device by changing the aggregation state of complex **1**.

Introduction

Vapochromic materials, which undergo reversible changes in colour and/or emission characteristics in response to volatile organic compounds (VOCs) have been widely investigated for their emerging applications in anti-counterfeit, data security and data recording devices.[1,2] For these vapochromic materials, the solid-state molecular packing modes can easily be altered by exposure to vapour due to changed intermolecular interactions.[3,4] Subsequently, the visible colour and the wavelengths and intensities of emission bands can be drastically altered. However, achieving stable vapochromic behaviour is still an important issue to be solved.[5] For instance, some coordination and organometallic complexes restore their original colour and emission spectra in the presence of air or vacuum due to the evaporation of the VOCs to which they have been exposed.[6-8] Therefore, the development of vapochromic materials which possess stable and reversible optical changes is a particular challenge.

Piezochromic luminescent (PCL) materials are a class of functional materials which change colour or emission in the solid state in response to stimuli, such as external pressure or mechanical grinding.[9-12] Their different luminescent properties are attributed to variation of aggregation modes (crystalline or amorphous).[13,14] The original emission colour of the solids can be restored by recovering the initial molecular packing mode via recrystallization or heating.[15,16] In this regard, PCL materials can overcome the shortcomings of instability that is usual for vapochromic materials. Thus, PCL materials have applications in sensors, security materials, and information display/storage. Nevertheless, a drawback is that the synthesis of PCL compounds generally requires complex, multi-step procedures,[17] so a simple and easy approach to synthesize PCL materials is highly desirable.

Phosphorescent transition-metal complexes, especially Ir(III) systems, are widely studied in materials science due to their high luminescence quantum yields, ease of handling in laboratory conditions, structural versatility and high photostability.[18-21] Consequently, many phosphorescent sensors based on Ir(III) complexes utilize their sensitive and selective responses to environmental stimulus.[22-24] However, their propensity for strong intermolecular π-stacking and molecular rotation can make them readily aggregate, which in turn causes phosphorescence quenching at a high concentration or in the solid state.[25] In recent years, there has been a growing interest in materials which possess aggregation induced emission (AIE-active materials) as named by Tang et al. in 2001.[26] For AIE-active materials, emission intensities are significantly enhanced in the solid state where the intramolecular rotations which quench luminescence in dilute solutions can be efficiently restricted.[27-30] The attractive properties of AIE-active materials prompted us to consider potential luminescence sensing applications based on Ir(III) complexes through rational molecular design.

a. Key Laboratory of Nanobiosensing and Nanobioanalysis at Universities of Jilin Province, Department of Chemistry, Northeast Normal University, 5268 Renmin Street, Changchun, Jilin Province 130024, P.R. China. E-mail: zhudx047@nenu.edu.cn; zmsu@nenu.edu.cn
b. Department of Chemistry, Durham University, Durham, DH1 3LE, UK. E-mail: m.r.bryce@durham.ac.uk
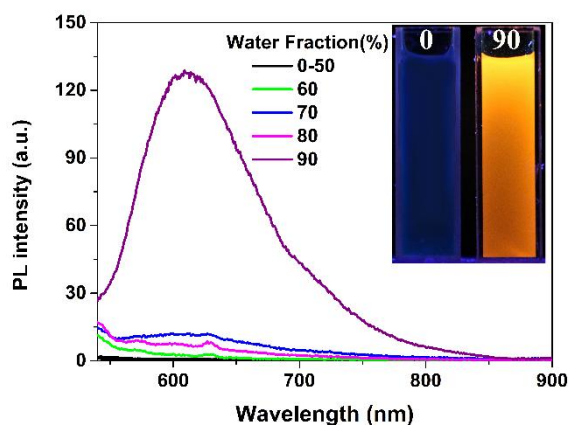
Fig. 1 Emission spectra of **1** in THF-water mixtures with different water fractions (0-90% v/v) at room temperature. Inset: emission image of **1** in pure THF solution and THF–water mixture (90% water fraction) under 365 nm UV illumination.

In the present work we employed a highly flexible Schiff base ligand to construct an AIE-active molecule with strong intermolecular interactions between the aryl rings in the aggregated or crystal state. Based on our recent work,[22] in which complex **PIBIP** showed poor solubility in organic solvents, in this article we have employed *t*-butyl substituents which have several important benefits. (i) The solubility of **1** is enhanced thereby extending the range of VOCs that can be exploited.[22,24, 31, 32] (ii) At the same time, the bulky *t*-butyl substituents are expected to improve the PCL the properties of complex **1** as steric repulsion should lead to a looser molecular stacking in crystal, in which the crystal structure could be destroyed easily by external force.[33] (iii) The AIE properties are also modified by the *t*-butyl groups because their presence can significantly enhance the degree of molecular distortion because of steric hindrance. They can reduce strong intermolecular π-stacking which can make the complex readily aggregate and quench emission at a high concentration or in the solid state.[34]

The multifunctional dinuclear Ir(III) complex **1** was synthesized in good yield from readily-available starting materials. The photophysical properties demonstrate that **1** is AIE-active and simultaneously shows PCL properties. Meanwhile, the emission characteristics of the ground sample can be converted back to those of the as-synthesized sample upon simple fuming by VOCs. On the basis of these findings, a reversible monitoring device for VOCs was fabricated exploiting the evident phosphorescence colour and intensity changes induced by mechanical grinding and fuming with VOCs.

Synthesis

Complex **1** was synthesized using the previously reported procedures.[35,22] The route is shown in Scheme 1. A yellow suspension of the dichloro-bridged diiridium complex [Ir(ppy)$_2$Cl]$_2$ (0.353 g, 0.33 mmol), bridging ligand **a** (0.141 g, 0.33 mmol) and Na$_2$CO$_3$ (0.349 g, 3.2 mmol) in 2-ethoxyethanol (30 ml) was stirred at 135 °C for 6 hours under a nitrogen atmosphere and the suspension was then filtered, the precipitate was washed with diethyl ether and water. Then the crude product was dried and
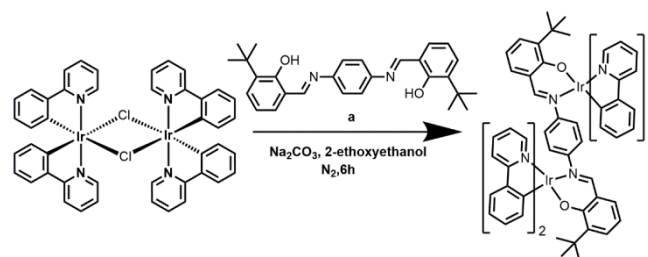
Scheme 1. Synthetic route to complex **1**.

purified by silica gel column chromatography with petroleum ether / dichloromethane (10:6 v/v) as eluent. **1** was obtained as an orange crystalline solid in 62% yield (0.291 g). ^{1}H NMR (500 MHz, CDCl$_3$, δ [ppm]): δ 8.76 (d, *J* = 5 Hz, 2H); 8.69 (d, *J* = 5 Hz, 2H); 7.81 (s, 2H); 7.78 (d, *J* = 7 Hz, 2H); 7.65 (t, *J* =7 Hz, 2H); 7.62 (t, *J* = 8 Hz, 2H); 7.54 (d, *J* = 7 Hz, 2H); 7.50 (d, *J* = 6 Hz, 2H); 7.11 (d, *J* = 5 Hz, 2H); 7.02 (d, *J* = 10 Hz, 8H); 6.81 (t, *J* = 7 Hz, 3H); 6.68 (t, *J* = 5 Hz, 3H); 6.59 (t, *J* = 7 Hz, 3H); 6.46 (t, *J* = 7 Hz, 3H); 6.34 (t, *J* = 6 Hz, 2H); 6.20 (d, *J* = 7 Hz, 2H); 6.11 (d, *J* = 7 Hz, 2H); 0.947 (s, 18H). MS: (MALDI-TOF) [m/z]: 1427.78 (calcd: 1428.42). Anal. Calcd. for C$_{72}$H$_{62}$Ir$_2$N$_6$O$_2$: C 53.65, H 4.14, N 5.01. Found C 53.58, H 4.11, N 5.06. Single crystals for X-ray analysis were grown by diffusion of ether into a solution of **1** in dimethyl sulfoxide.

Results and discussion

Since the pristine solid sample of **1** emits bright luminescence, the AIE properties were investigated by UV/vis absorption and emission spectroscopy in a THF/water mixed solvent system with varying amounts of water at room temperature. As shown in Fig 1, the emission band of **1** in dilute THF is not detectable. Nevertheless, the phosphorescence emission of **1** is dramatically enhanced at around 609 nm when 90% (v/v) of distilled water is added and the corresponding PL intensity increased by up to about 168-fold in comparison with the data at 0% water fraction. To further investigate the cause of the AIE behaviour of **1**, absorption spectra and transmission electron microscope (TEM) studies were performed on the THF solution of **1** with different water fractions. As shown in Fig. S2, when the water fraction increases from 60 to 90%, the absorption bands rise in intensity and shift to longer wavelengths. Meanwhile, the spectra are almost identical in pure THF solution and 50% THF/water mixtures. Evidence for aggregates of **1** in the solvent mixture is seen in the level-off tail in the visible spectral region; such tails are a signature of nanoparticle suspensions.[36] Meanwhile, TEM shows that spherical nano-aggregates emerge with the increasing proportion of water in the THF/water mixture (Fig. S3, ESI†).[37] All the above results confirm that **1** is an AIE-active chromophore.

Density Functional Theory (DFT) calculations have been carried out to investigate the originally weak emission for **1** in the solution state. The optimized geometries of complex **1** at the S$_0$ and T$_1$ states in solution are shown in Figure S6. The selected calculated bond lengths, bond angles and dihedral angles at both the optimized ground state (S$_0$) and triplet excited state (T$_1$) for **1** are shown in Table S2 (ESI†). Large structural distortions are found in the T$_1$ geometry compared to the S$_0$ geometry which induce a larger excited-state relaxation and may result in an effective pathway for
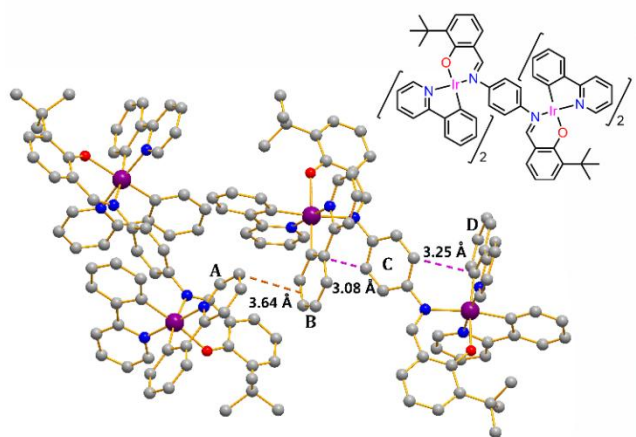
Fig. 2 The structural formula and X-ray crystal structure of **1** showing intermolecular (A---B) and intramolecular (B---C) and (C---D) π–π interactions. Colour code: Ir purple; N blue; O red; C grey; H atoms are omitted

Fig. 3 (a-b) Emission spectra of "as prepared" (not ground) sample (**P**), ground sample (**G**), ground sample after exposure to DCM solvent vapour (**S**) and heated ground sample (**H**). Inset: Emission image of **P** and **G** under 365 nm UV illumination. (c) Emission spectra of **P** after exposure to CH_2Cl_2 (**P$_1$**) and **G** after exposure to corresponding solvent (CH_2Cl_2, $CHCl_3$, THF, Acetone and MeOH) and further grinding (**G$_1$**, **G$_2$**, **G$_3$**, and **G$_4$**). (d) Maximum emission wavelength of **1** through five cycles of states **G** and **S** in response to the corresponding vapour of a range of VOCs.

nonradiative decay, which can explain the weak emission for **1** in the solution state. Furthermore, the low temperature (77 K) luminescence for **1** in the dilute solution shows bright emission with λ_{max} at 610 nm (Fig. S4, ESI†). Thus, the mechanism of AIE is attributed to the restriction of intramolecular motion (RIM).[28-30]

To gain more insight into the molecular structure of **1**, X-ray crystallographic analysis revealed that in the unit cell two crystallographically independent molecules interact with each other through intermolecular π (pyridine)–π (benzene ring) interactions (Fig. 2). Meanwhile, intramolecular π–π interactions exist between the bridging phenyl ring and the adjacent phenyl rings of phenylpyridine. The dihedral angles between the planes of pyridyl and phenyl rings is 22° (A---B). The dihedral angles between the planes of the two phenyl rings were observed to be 19° (B---C) and 34° (C---D), respectively (Fig. S7, ESI†). As a result, extended molecular chains are constituted through close π–π stacking in the crystal structure. It is known that intermolecular or intramolecular π–π interactions can be easily modified when mechanical pressure is applied, and thus resulting in PCL phenomena.[9] In this regard, we envisaged that piezochromism might be realised in **1**. Therefore, the emission spectra of the "as-prepared" samples (abbreviated as **P**) and the samples which were thoroughly ground by hand in an agate mortar (ground samples **G**) were recorded. As depicted in Fig. 3a and 3b, the sample **P** shows orange phosphorescence. After thoroughly grinding for 30 s, the emission maxima of **P** is red-shifted from 608 nm to 624 nm and the emission intensity of the sample is dramatically reduced, as is clearly visible to the naked eye. This phenomenon is in accordance with the photoluminescence quantum yield (PLQY) which decreased significantly after grinding from 24% (**P**) to 0.05% (**G**) (Table S1, ESI†). This **G**-form solid gave the **P**-form powder again within a few seconds when exposed to dichloromethane (DCM) solvent vapour (abbreviated as **S**). This is a typical example of
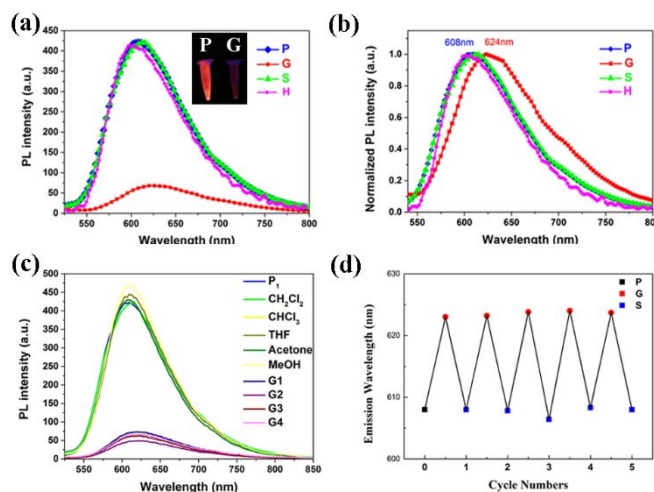
reversible piezochromic luminescence. Consistent with the previous literature regarding AIE-active piezochromic materials.[38]

Remarkably, the **S**-form of **1** is extremely stable, and the phosphorescent properties remain almost unchanged in air for several months at room temperature. Even after the removal of DCM vapour molecules under vacuum for 1 week, the phosphorescence persisted without any obvious change. This ultra-high stability clearly differs from the properties reported for many vapochromic systems, including an analogue of **1**,[22] which recover their original colour quickly when the organic vapours are removed in air or vacuum. To investigate the origin of reversible PCL behavior of **1**, the following analyses were carried out. The ^{1}H NMR spectra of both **P** and **G** show similar peak shapes and chemical shift values (Fig. S1, ESI†) which demonstrate that there is a physical process, rather than a chemical reaction, occuring in the grinding process. Since the photophysical properties of organic molecules are correlated with their aggregation state, powder X-ray diffraction (PXRD) was carried out to determine the phase characteristics of **1**. As shown in Fig. 4a, **P** showed intense and sharp reflection peaks, indicating that molecules of **1** in the **P**-form pack to give a relatively well-defined microcrystalline-like structure. However, on the contrary, the **G**-form solid does not show any noticeable diffraction in the XRD profile. The result indicates that the crystalline-like ordered structure of the **P**-form has been disrupted in the **G**-form solid. After heating (**H**) or exposing **G** to DCM vapour some sharp diffraction peaks reappeared, confirming that **G** readily recrystallizes by heating or fuming. The product after recrystallization is stable and thus can retain the phosphorescent properties for a longer time than other traditional vapochromic materials. Differential scanning calorimetry (DSC) traces further
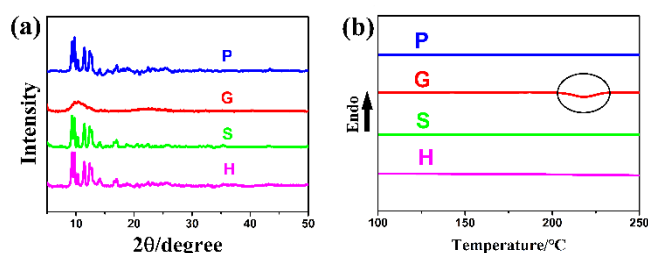
Fig. 4 Powder X-ray diffraction patterns (a) and the DSC traces (b) of the corresponding samples.

confirm this PCL mechanism. Upon heating **G** to 250 ^{o}C, the DSC traces exhibited a clear broad exothermic recrystallization peak at ca. 210 ^{o}C (Fig. 4b). Nevertheless, the samples of **P, S** and **H** exhibited no melting endothermic peak in their DSC profiles (Fig. 4b). Thus, these results confirm that the ground sample **G** is amorphous and its thermal recrystallization temperature is ca. 210 ^{o}C, and that after fuming by DCM solvent vapour or heating, **G** reverts to **P** and consequently its phosphorescent properties are identical with those originally observed. In conclusion, all the above results suggest that the reversible piezochromic properties of **1** can be attributed to the phase transformation between crystalline state and amorphous states. Before grinding, there exists the orderly molecular arrangement, because of the presence of inter and intra-molecular π-π interactions. Upon grinding, the resultant amorphous sample stacked in a smaller slippage packing mode which is possibly attributed to the flexible imine units of the Schiff base bridging ligand.[9, 39]

Combining the high contrast and rapid switching ability of PCL with the aforementioned AIE properties of **1**, a chemical monitor device for detecting volatile organic compounds (VOCs) was fabricated. The detailed experiment is as follows. The starting warning signal is composed of powder **G** which emits weak red phosphorescence upon illumination with a 365 nm UV lamp. It is carefully spread on a filter paper using a porcelain pestle to make a thin film. Then the warning signal is placed on beakers containing VOCs (10 ml) to adsorb organic vapour. The vapour can switch the device ON or OFF by altering the aggregation state between crystalline and amorphous (Fig. 5). A large family of VOC vapours are shown to act as switches to turn on this monitor rapidly from a weakly red-emitting state to an intensely strong orange-emitting state (named the WARNING state, with an exclamation mark symbol). Upon further grinding this signal disappeared and the original emission property of **G** was regenerated indicating that the monitor was now in the ALL-CLEAR state and ready to provide a new cycle of detection. Notably, the different states can be easily distinguished by the colour and emission properties of the sample. In addition, when the warning signal was exposure to non-solvents of **1**, such as *n*-hexane, petroleum ether (PE) and diethyl ether, no phosphorescent change can be observed. However, when the red-emitting signal was exposed to good solvents of **1**, such as chloroalkanes (CH_2Cl_2, $CHCl_3$, CH_2ClCH_2Cl), tetrahydrofuran (THF), ethyl acetate and acetone, the red-emitting signal underwent an obvious change of its phosphorescence within 10 s. Furthermore, acetonitrile and methanol required approximately 30 s and 1 min, respectively, because they are relatively poor solvents of **1**. The XRD and DSC traces prove that this behaviour is attributed to the vapours of the good solvents readily disturbing the amorphous

Fig. 5 Photographic images under illumination with UV light of the monitoring of VOCs by **1** after exposure to different VOCs and grinding.

packing in **G** and inducing recrystallizations accompanied by a change of emission colour (Fig. S5, ESI†).[1] Therefore, there is an efficient distinction among different VOCs by comparison of the extent of the change and the time required to achieve the change. The solvent vapours with higher polarities, such as $CHCl_3$ and MeOH, significantly increase the response, while the solvents with low polarities, such as *n*-hexane, do not induce recrystallization and therefore do not trigger a response. It is noteworthy that when **G** was exposed to different solvent vapours, the emission spectra can revert to the original spectra of **P** within a few seconds. After further grinding, the emission spectra of **G** is recovered. These results demonstrate that the reversibility of **1** is excellent and the repeatability of amorphization and crystallization by grinding–fuming cycles leads to almost no change of emission colour or loss of intensity (Fig. 3c and d). On the basis of these findings, complex **1** has the potential to be employed in practical applications as a monitor of VOCs with good selectivity, fast response time and a clear photophysical read-out of a warning signal.

Conclusions

In summary, a new Ir(III) complex **1** containing a Schiff base ligand has been synthesized and shown to act as a multifunctional and switchable material. We have demonstrated that **1** exhibits AIE, highly reversible piezochromic and vapochromic properties. It is proposed that the conformationally flexible Schiff base bridging ligand plays an important role in achieving AIE and PCL properties simultaneously. In relation to the piezochromic and vapochromic properties, the emission bands of **1** and their intensity are dramatically changed by switching the aggregation state between the crystalline and the amorphous states. These combined properties have allowed a simple monitor for VOCs to be fabricated, which can respond to relatively high polarity solvents with different response times. Thus, the monitor developed in this work extends the current VOC sensing technology and can be used to selectively detect the leakage of VOCs, such as chloroalkanes, tetrahydrofuran

and ethyl acetate. Complex **1** presents a viable strategy for designing switchable PCL materials with real-time monitoring properties.

Acknowledgements

Notes and references

1. C. Ge, Y. Liu, X. Ye, X. Zheng, Q. Han, J. Liu and X. Tao, *Mater. Chem. Front.*, 2017, **1**, 530-537.
2. B. Jiang, J. Zhang, J. Q. Ma, W. Zheng, L. J. Chen, B. Sun, C. Li, B. W. Hu, H. Tan, X. Li and H. B. Yang, *J. Am. Chem. Soc.*, 2016, **138**, 738-741.
3. T. Yu, D. Ou, L. Wang, S. Zheng, Z. Yang, Y. Zhang, Z. Chi, S. Liu, J. Xu and M. P. Aldred, *Mater. Chem. Front.*, 2017, **1**, 1900-1904.
4. B. R. Varju, J. S. Ovens and D. B. Leznoff, *Chem. Commun.*, 2017, **53**, 6500-6503.
5. Y. Qin, J. Shi, X. Gong, Z. Tian, P. Zhang and J. Lu, *Adv. Funct. Mater.*, 2016, **26**, 6752-6759.
6. S. H. Lim, M. M. Olmstead and A. L. Balch, *J. Am. Chem. Soc.*, 2011, **133**, 10229-10238.
7. Y. Q. Sun, Y. L. Lei, J. Gao, X. H. Sun, S. H. Lin, Q. L. Bao, Q. Liao, S. T. Lee and L. S. Liao, *Chem. Commun.*, 2014, **50**, 10812-10814.
8. J. R. Berenguer, E. Lalinde, A. Martin, M. T. Moreno, S. Ruiz, S. Sanchez and H. R. Shahsavari, *Chem. Commun.*, 2013, **49**, 5067-5069.
9. G. Li, X. Ren, G. Shan, W. Che, D. Zhu, L. Yan, Z. Su and M. R. Bryce, *Chem. Commun.*, 2015, **51**, 13036-13039.
10. A. Pucci, R. Bizzarri and G. Ruggeri, *Soft Matter*, 2011, **7**, 3689.
11. A. Pucci, F. Di Cuia, F. Signori and G. Ruggeri, *J. Mater. Chem.*, 2007, **17**, 783-790.
12. S. Hirata and T. Watanabe, *Adv. Mater.*, 2006, **18**, 2725-2729.
13. Y. Dong, J. W. Y. Lam, A. Qin, J. Liu, Z. Li, B. Z. Tang, J. Sun and H. S. Kwok, *Appl. Phys. Lett.*, 2007, **91**, 011111.
14. Y. Sagara, T. Mutai, I. Yoshikawa and K. Araki, *J. Am. Chem. Soc.*, 2007, **129**, 1520-1521.
15. P. Galer, R. C. Korosec, M. Vidmar and B. Sket, *J. Am. Chem. Soc.*, 2014, **136**, 7383-7394.
16. Z. Song, R. Liu, Y. Li, H. Shi, J. Hu, X. Cai and H. Zhu, *J. Mater. Chem. C*, 2016, **4**, 2553-2559.
17. C. Ma, B. Xu, G. Xie, J. He, X. Zhou, B. Peng, L. Jiang, B. Xu, W. Tian, Z. Chi, S. Liu, Y. Zhang and J. Xu, *Chem. Commun.*, 2014, **50**, 7374-7377.
18. S. Lamansky, P. Djurovich, D. Murphy, F. Abdel-Razzaq, H.-E. Lee, C. Adachi, P. E. Burrows, S. R. Forrest and M. E. Thompson, *J. Am. Chem. Soc.*, 2001, **123**, 4304-4312.
19. M. Mydlak, C. Bizzarri, D. Hartmann, W. Sarfert, G. Schmid and L. De Cola, *Adv. Funct. Mater.*, 2010, **20**, 1812-1820.
20. H. Sasabe, J. Takamatsu, T. Motoyama, S. Watanabe, G. Wagenblast, N. Langer, O. Molt, E. Fuchs, C. Lennartz and J. Kido, *Adv. Mater.*, 2010, **22**, 5003-5007.
21. M. A. Baldo, D. F. O'Brien, Y. You, A. Shoustikov, S. Sibley, M. E. Thompson and S. R. Forrest, *Nature*, 1998, **395**, 151-154.
22. Y. Jiang, G. Li, W. Che, Y. Liu, B. Xu, G. Shan, D. Zhu, Z. Su and M. R. Bryce, *Chem. Commun.*, 2017, **53**, 3022-3025.
23. G. G. Shan, H. B. Li, H. T. Cao, D. X. Zhu, P. Li, Z. M. Su and Y. Liao, *Chem. Commun.*, 2012, **48**, 2000-2002.
24. Y. Han, H.-T. Cao, H.-Z. Sun, Y. Wu, G.-G. Shan, Z.-M. Su, X.-G. Hou and Y. Liao, *J. Mater. Chem. C*, 2014, **2**, 7648-7655.
25. R. Jakubiak, C. J. Collison, W. C. Wan and L. J. Rothberg, *J. Phys. Chem. A*, 1999, **103**, 2394-2398.
26. J. Luo, Z. Xie, J. W. Y. Lam, L. Cheng, B. Z. Tang, H. Chen, C. Qiu, H. S. Kwok, X. Zhan, Y. Liu and D. Zhu, *Chem. Commun.*, 2001, **1**, 1740-1741.
27. J. Mei, Y. Hong, J. W. Lam, A. Qin, Y. Tang and B. Z. Tang, *Adv. Mater.*, 2014, **26**, 5429-5479.
28. J. Yang, J. Huang, Q. Li and Z. Li, *J. Mater. Chem. C*, 2016, **4**, 2663-2684.
29. J. Mei, N. L. Leung, R. T. Kwok, J. W. Lam and B. Z. Tang, *Chem. Rev.*, 2015, **115**, 11718-11940.
30. Q. Li and Z. Li, *Sci. China Chem.*, 2015, **58**, 1800-1809.
31. Y. Han, H.-T. Cao, H.-Z. Sun, G.-G. Shan, Y. Wu, Z.-M. Su and Y. Liao, *J. Mater. Chem. C*, 2015, **3**, 2341-2349.
32. S. P. Anthony, *ChemPlusChem*, 2012, **77**, 518-531.
33. M. Liu, L. Zhai, J. Sun, P. Xue, P. Gong, Z. Zhang, J. Sun and R. Lu, *Dyes and Pigments*, 2016, **128**, 271-278.
34. Y. Zhan, Y. Xu, P. Yang, H. Zhang, Y. Li and J. Liu, *Tetrahedron Lett.*, 2016, **57**, 5385-5389.
35. K. A. King, P. J. Spellane and R. J. Watts, *J. Am. Chem. Soc.*, 1985, **107**, 1431-1432.
36. Ben Zhong Tang, Yanhou Geng, Jacky Wing Yip Lam and B. Li, *Chem. Mater.*, 1999, **11**, 1381-1389.
37. G. G. Shan, H. B. Li, J. S. Qin, D. X. Zhu, Y. Liao and Z. M. Su, *Dalton Trans.*, 2012, **41**, 9590-9593.
38. Z. Chi, X. Zhang, B. Xu, X. Zhou, C. Ma, Y. Zhang, S. Liu and J. Xu, *Chem. Soc. Rev.*, 2012, **41**, 3878-3896.
39. C. Wang and Z. Li, *Mater. Chem. Front.*, 2017, DOI: 10.1039/C7QM00201G.

Supporting Information

An AIE-active phosphorescent Ir(III) complex with piezochromic luminescence (PCL) and its application for monitoring volatile organic compounds (VOCs)

Yang Jiang,[a] Guangfu Li,[a] Dongxia Zhu,*[a] Zhongmin Su,*[a] Martin R. Bryce*[b]

[a.] *Key Laboratory of Nanobiosensing and Nanobioanalysis at Universities of Jilin Province, Department of Chemistry, Northeast Normal University, 5268 Renmin Street, Changchun, Jilin Province 130024, P.R. China. E-mail:* zhudx047@nenu.edu.cn; zmsu@nenu.edu.cn
[b.] *Department of Chemistry, Durham University, Durham, DH1 3LE, UK. E-mail:* m.r.bryce@durham.ac.uk

Contents:

1. Experimental - general information

2. ^{1}H NMR spectra of **1** at room temperature

3. Photophysical properties

4. Quantum Chemical Calculations

5. X-ray crystallographic data

6. References

1. Experimental - general information

Materials obtained from commercial suppliers were used without further purification unless otherwise stated. All glassware, syringes, magnetic stirring bars, and needles were thoroughly dried in a convection oven. Reactions were monitored using thin layer chromatography (TLC). Commercial TLC plates were used and the spots were visualised under UV light at 254 and 365 nm. ^{1}H NMR spectra were recorded at 25 ℃ on a Varian 500 MHz spectrometer. The chemical shifts (δ) are given in parts per million relative to internal standard TMS. The ^{1}H NMR spectra were referenced internally to the residual proton resonance in $CDCl_3$ (δ 7.24 ppm). Powder X-ray diffraction (XRD) patterns of the samples were collected on a Rigaku Dmax 2000. Differential scanning calorimetry (DSC) curves were obtained with a NETZSCH thermal analysis DSC200 F_3 under argon with a heating rate 10 °C min^{-1}. Transmission electron microscopy (TEM) and electron diffraction analyses of the samples were obtained using a TECNAI F20 microscope. The samples were prepared by placing microdrops of the solution on a holey carbon copper grid. UV-vis absorption spectra were recorded on a Shimadzu UV-3100 spectrophotometer. Photoluminescence spectra were collected on a Shimadzu RF-5301pc spectrophotometer and Maya 2000Pro optical fiber spectrophotometer. PL efficiencies were measured with an integrating sphere (C-701, Labsphere Inc.) with a 365 nm Ocean Optics LLS-LED as the excitation source, and the laser was introduced into the sphere through an optical fiber. The excited-state lifetimes were measured by exciting the samples with 385 nm light pulses with ~3 ns pulse width from a Quanty-Ray DCR-2 pulsed Nd: YAG laser. The X-ray crystal structure data of complex **1** were collected on a Bruker Smart Apex II CCD diffractometer with graphite-monochromated Mo Kα radiation ($\lambda = 0.71069$ Å) at room temperature.

Warning signal manufacturing method

The warning signal adopted the shape of a 'triangle' comprising a central 'exclamation mark'. A specific mould (filter paper with holes) was made for regulating the shape of as-prepared powder **G**. **G** was carefully spread within the hole and the filter paper removed so that the whole warning signal can be demonstrated.
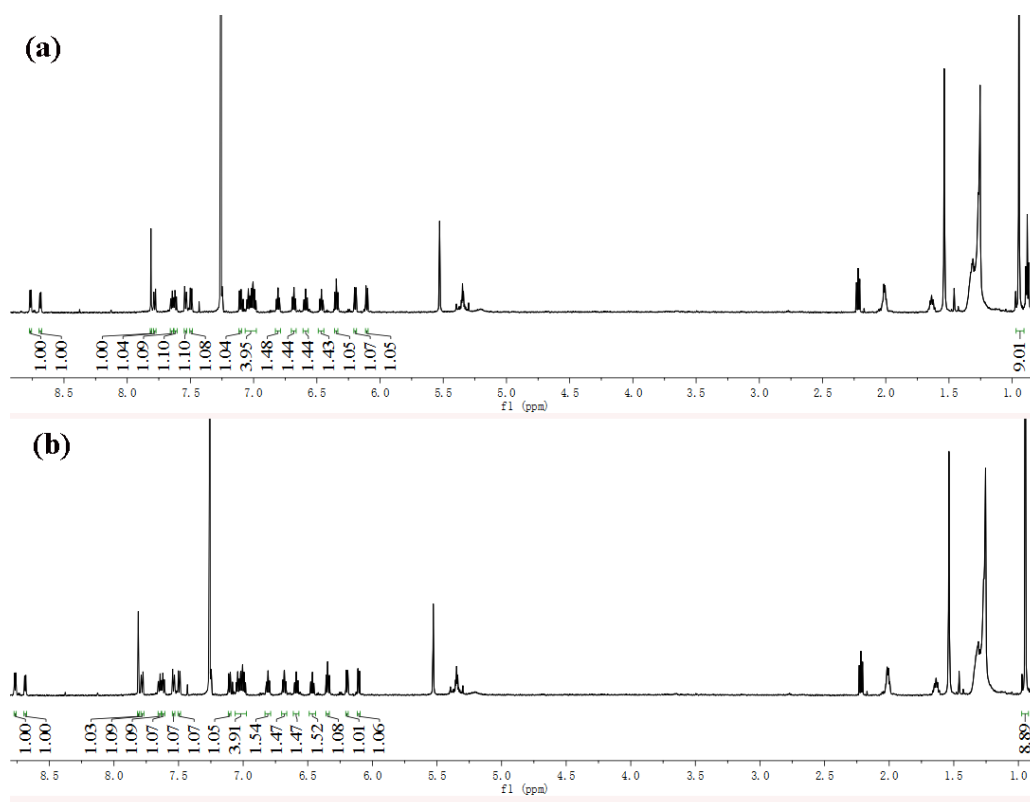
2. ^{1}H NMR Spectra of 1 at room temperature

(a)

(b)

Fig. S1 ^{1}H NMR spectra of **1** in $CDCl_3$ before grinding (a) and after grinding (b).

3. Photophysical properties

Table S1 The phosphorescent emission efficiency (Φ_{em}) and excited-state lifetimes (τ) in various states of **1**.

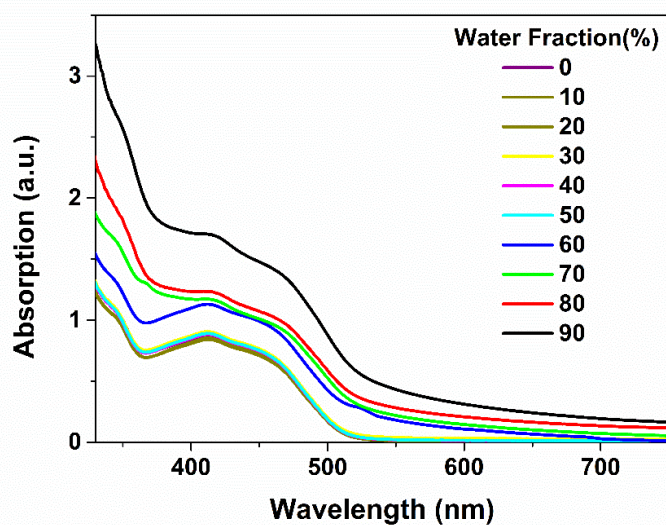|	As-prepared (P)	Ground (G)	CH$_2$Cl$_2$ fumed (D)	Heated (H)
Φ_{em}	0.24	0.05	0.26	0.31
τ (µs)	0.67	1.54	0.61	0.64

Fig. S2 UV-visible absorption spectra of **1** in THF-water mixtures with different water fractions (0-90%, v/v) at room temperature.
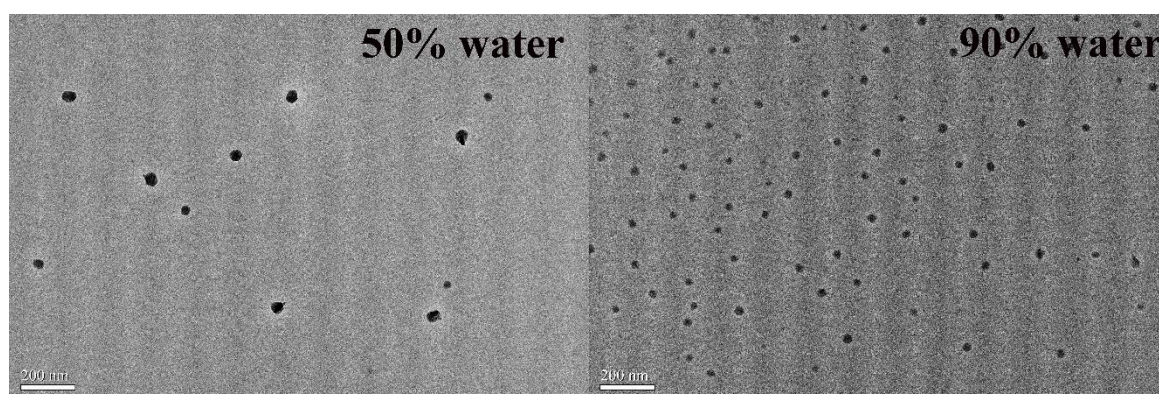

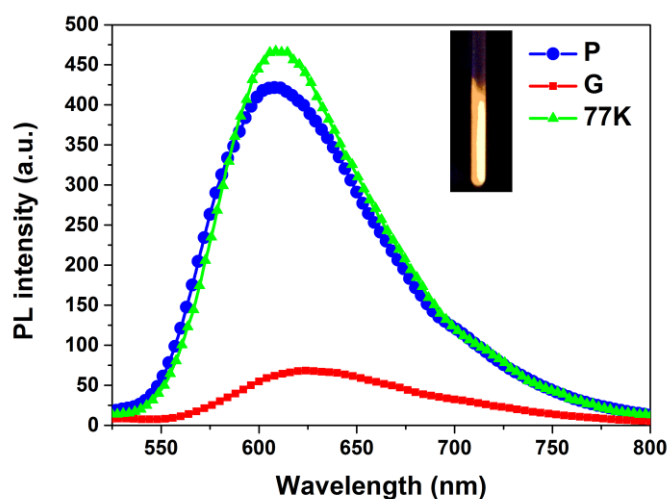**Fig. S3** TEM image of nanoaggregates of **1** formed in THF–H₂O mixtures with 50% (left) and 90% (right) water fraction.

Fig. S4 Emission spectra of **1** in THF solution (10^{-5} mol/L) at 77 K, "as prepared" sample (**P**) and ground sample (**G**), respectively.
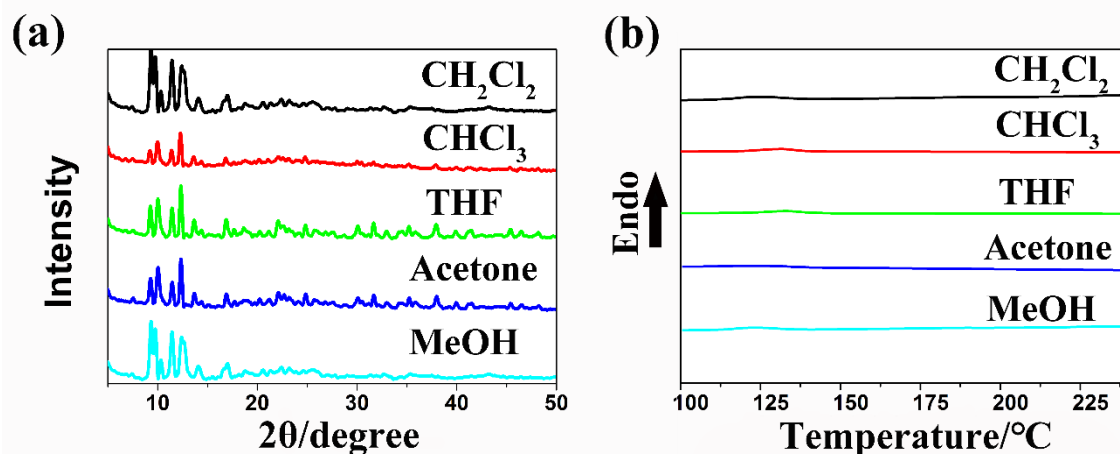
Fig. S5 Powder X-ray diffraction patterns (a) and the DSC traces (b) of **G** after exposure to the corresponding solvent (CH_2Cl_2, $CHCl_3$, THF, Acetone and MeOH).

4. Quantum Chemical Calculations

All calculations were performed with the Gaussian 09 program package.[1] The B3LYP functional was employed for all DFT calculations. The 6-31G* basis set was employed for H, C, N, O atoms, while the iridium atom was described by the Hay-Wadt effective core potential (ECP) and a double-ξ basis set LANL2DZ. Full geometry optimisation with C1 symmetry constraints was carried out in solution for the singlet ground state (S_0) of complex **1**. A solvent effect was taken into account by the polarisable continuum model (PCM) with tetrahydrofuran (THF) as solvent.
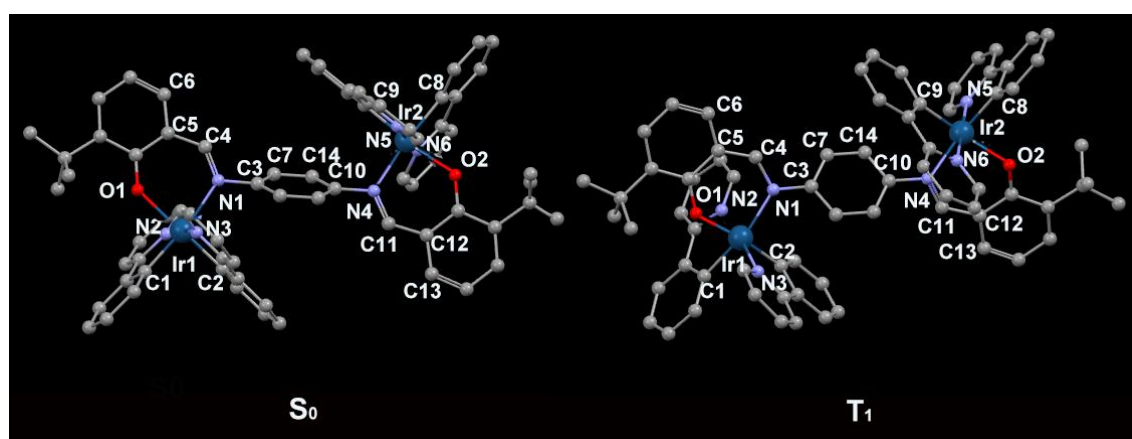

Fig. S6 Optimised geometries of complex **1** at S_0 and T_1 states in solution state.

Table S2 Selected calculated bond lengths (Å), bond angles (º) and dihedral angles (º) at both optimized S_0 and T_1 geometries for complex **1**.

1	T_1	S_0
Ir1-N1	2.232	2.23
Ir1-N2	2.068	2.067
Ir1-N3	2.077	2.078
Ir1-C1	2.019	2.02
Ir1-C2	2.014	2.014
Ir1-O1	2.189	2.192
C1-Ir1-N1	173.62	173.82
C2-Ir1-O1	173.95	174.01
N2-Ir1-N3	176.39	176.17
C2-Ir1-C1	88.49	88.53
C3-N1-C4	115.38	115.51
C5-C4-N1	130.99	130.6
Ir1-N1-C4-O1	0.95	3.4
C6-C5-C4-N1	7.13	9.31
C7-C3-N1-C4	52.18	56.42
Ir2-N4	2.211	2.234
Ir2-N5	2.06	2.065
Ir2-N6	2.095	2.085
Ir2-C8	2.034	2.022
Ir2-C9	2.012	2.013
Ir2-O2	2.17	2.195
C8-Ir2-N2	170.79	172.61
C9-Ir2-O2	173.2	173.88
N5-Ir2-N6	172.12	174.09
C9-Ir2-C8	88.03	88.77
C10-N2-C11	115.17	114.92
C12-C11-N2	129.9	130.8
Ir2-N2-C11-O2	19.67	7.72
C13-C12-C11-N2	2.22	4.95
C14-C10-N2-C11	143	116.77

5. X-ray crystallographic data

The molecular structure of **1** was confirmed by X-ray crystallographic analysis of single crystals. Diffraction data were collected on a Bruker SMART Apex CCD diffractometer using k(Mo-Kα) radiation (k = 0.71069 Å). Cell refinement and data reduction were made by the SAINT program. The structure was determined using the SHELXTL/PC program. The crystallographic data have been deposited with the Cambridge Crystallographic Data Centre with CCDC deposition number 1571781. These data can be obtained free of charge from The Cambridge Crystallographic Data Centre via www.ccdc.cam.ac.uk/data_request/cif.
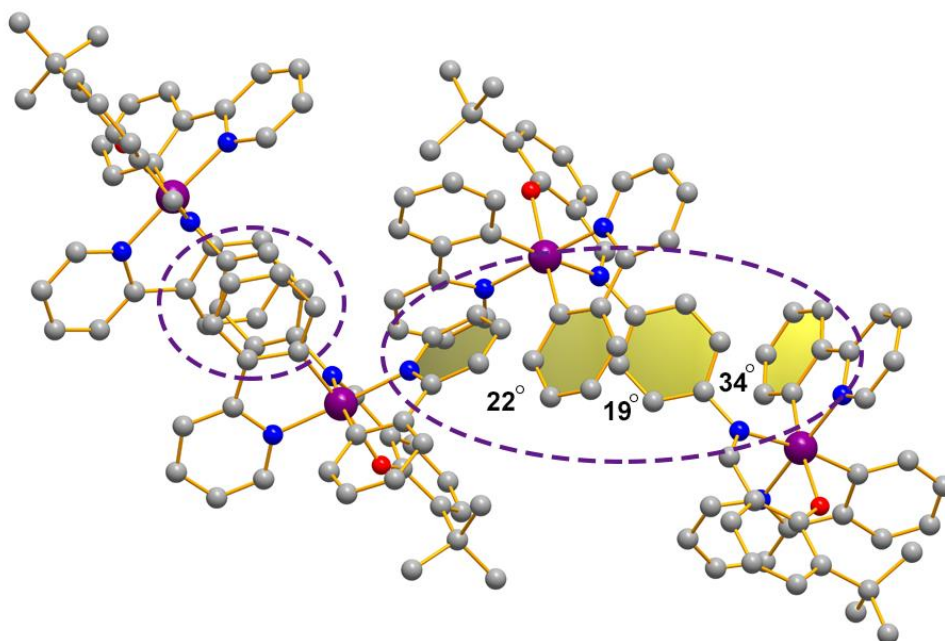
Fig. S7 Molecular packing of **1** in the crystal. Colour code: Ir purple; N blue; O red ; C grey; H atoms are omitted for clarity. The dihedral angles are 22°, 19° and 34°, respectively**.**

Table S3 Crystal data and structure refinement for complex **1**.

	Complex 1
Empirical formula	$C_{72}H_{62}Ir_2N_6O_2$
Formula weight	1428.42
Temperature (K)	293(2)
Crystal system	Monoclinic
Space group	P2(1)/c
a/Å	19.8730(14)
b/ Å	12.8050(8)
c/ Å	28.261(2)
α/°	90.00
β/°	103.880(3)
γ/°	90.00
V/ Å^3	6981.7(8)
Z	4
P_{calc}(g/cm^3)	1.404
μ/mm^{-1}	3.858
R_{int}	0.0636
Goodness-of-fit on F^2	1.114
R_1[a],wR_2[b][I>2σ(I)]	0.0690, 0.1942
R_1,wR_2(all data)	0.1201, 0.2406

[a]$R_1 = \Sigma\ ||Fo|-|Fc||/\ \Sigma\ |Fo|$. [b]$wR_2 = \{\ \Sigma\ [w(Fo^2-Fc^2)^2]/\ \Sigma\ [w(Fo^2)^2]\}^{1/2}$

6. References

1. M. J. Frisch, G.W. Trucks, H. B. Schlegel, G. E. Scuseria, M. A. Robb, J. R. Cheeseman, G. Scalmani, V. Barone, B. Mennucci, G. A. Petersson, H. Nakatsuji, M. Caricato, X. Li, H. P. Hratchian, A. F. Izmaylov, J. Bloino, G. Zheng, J. L. Sonnenberg, M. Hada, M. Ehara, K. Toyota, R. Fukuda, J. Hasegawa, M. Ishida, T. Nakajima, Y. Honda, O. Kitao, H. Nakai, T. Vreven, J. A. Montgomery, Jr., J. E. Peralta, F. Ogliaro, M. Bearpark, J. J. Heyd, E. Brothers, K. N. Kudin, V. N. Staroverov, R. Kobayashi, J. Normand, K. Raghavachari, A. Rendell, J. C. Burant, S. S. Iyengar, J. Tomasi, M. Cossi, N. Rega, J. M. M. Millam, M. Klene, J. E. K. Knox, J. B. C. Cross, V. Bakken, C. Adamo, J. Jaramillo, R. Gomperts, R. E. Stratmann, O. Yazyev, A. J. Austin, R. Cammi, C. Pomelli, J. W. Ochterski, R. L. Martin, K. Morokuma, V. G. Zakrzewski, G. A. Voth, P. Salvador, J. J. Dannenberg, S. Dapprich, A. D. Daniels, O. Farkas, J. B. Foresman, J. V. Ortiz, J. Cioslowski and D. J. Fox, Gaussian 09, Revision A.02, Gaussian, Inc, Wallingford CT, **2009**.